# Charge transfer induced Lifshitz transition and magnetic symmetry breaking in ultrathin CrSBr crystals

Marco Bianchi [1], Kimberly Hsieh [1], Esben Juel Porat,[1] Florian Dirnberger [2], Julian Klein,[3] Kseniia Mosina,[4]
Zdenek Sofer,[4] Alexander N. Rudenko [5], Mikhail I. Katsnelson [5], Yong P. Chen,[1,6]
Malte Rösner [5,*] and Philip Hofmann [1,†]

[1]*Department of Physics and Astronomy, Interdisciplinary Nanoscience Center (iNANO), Aarhus University, 8000 Aarhus C, Denmark*
[2]*Institute of Applied Physics and Würzburg-Dresden Cluster of Excellence ct.qmat, Technische Universität Dresden, 01069 Dresden, Germany*
[3]*Department of Materials Science and Engineering, Massachusetts Institute of Technology, Cambridge, Massachusetts 02139, USA*
[4]*Department of Inorganic Chemistry, University of Chemistry and Technology Prague, Technicka 5, 166 28 Prague 6, Czech Republic*
[5]*Institute for Molecules and Materials, Radboud University, 6525 AJ Nijmegen, The Netherlands*
[6]*Department of Physics and Astronomy and Purdue Quantum Science and Engineering Institute,
Purdue University, West Lafayette, Indiana 47907, USA*

Ultrathin CrSBr flakes are exfoliated *in situ* on Au(111) and Ag(111) and their electronic structure is studied by angle-resolved photoemission spectroscopy. The thin flakes' electronic properties are drastically different from those of the bulk material and also substrate dependent. For both substrates, a strong charge transfer to the flakes is observed, partly populating the conduction band and giving rise to a highly anisotropic Fermi contour with an Ohmic contact to the substrate. The fundamental CrSBr band gap is strongly renormalized compared to the bulk. The charge transfer to the CrSBr flake is substantially larger for Ag(111) than for Au(111), but a rigid energy shift of the chemical potential is insufficient to describe the observed band structure modifications. In particular, the Fermi contour shows a Lifshitz transition, the fundamental band gap undergoes a transition from direct on Au(111) to indirect on Ag(111) and a doping-induced symmetry breaking between the intralayer Cr magnetic moments further modifies the band structure. Electronic structure calculations can account for nonrigid Lifshitz-type band structure changes in thin CrSBr as a function of doping and strain. In contrast to undoped bulk band structure calculations that require self-consistent *GW* theory, the doped thin film properties are well approximated by density functional theory if local Coulomb interactions are taken into account on the mean-field level and the charge transfer is considered.

## I. INTRODUCTION

The physics of two-dimensional (2D) magnetism is fascinating in its own right [1–5], and the recent realization of 2D magnetic materials not only gives ample opportunity to investigate the fundamental principles of 2D magnetism, it also provides the technology for integrating magnetism into 2D materials-based devices via proximity exchange effects [6]. Prominent examples of exfoliated 2D ferromagnets are $CrI_3$ [7], $Cr_2Ge_2Te_6$ [8], $Fe_3GeTe_2$ [9], and CrSBr [10,11]. CrSBr stands out because of a high Curie and Néel temperature for intralayer ferromagnetic and interlayer antiferromagnetic ordering, respectively (150 and 132 K) [10,11]. Its magnetic properties are stabilized by an orthorhombic crystal structure that has been theoretically predicted to lead to highly anisotropic bands in the lowest conduction bands, with strongly one-dimensional (1D)-like characteristics [12–17]. The theoretical description of the bulk properties is highly challenging due to the need to account for magnetism (including disorder and paramagnetism in the high-temperature phase), electronic correlations, and long-range Coulomb interactions [17,18].

So far, the predicted anisotropic electronic states in the conduction band (CB) have only been observed indirectly via optical and transport properties in the bulk and down to single layers [11,19,20]. The bulk band structure in the paramagnetic phase has been determined by angle-resolved photoemission spectroscopy (ARPES) [17] but this does not give access to the CB in a semiconductor.

Here we apply the recently introduced kinetic single-layer synthesis (KISS) technique [21] to prepare ultrathin flakes of CrSBr on Au(111) and Ag(111) substrates *in situ* with an atomically clean interface. Surprisingly, this leads to a giant charge transfer to the CrSBr flakes and a partial CB filling. This gives rise to an Ohmic contact between the materials, makes the anisotropic lowest CB directly accessible to ARPES measurements, and it induces an intralayer magnetic symmetry breaking. Given their metallicity, the thin films can also be measured at low temperatures, solving the problem of charging that can be an issue for magnetic semiconductors [17,22].

*m.roesner@science.ru.nl
†philip@phys.au.dk

## II. METHODS

CrSBr crystals are synthesized by chemical vapor transport growth [19]. ARPES experiments are performed at the SGM-3 beam line of ASTRID2 [23]. The sample temperature is 35 K unless specified otherwise. The synchrotron radiation polarization and the sample-to-analyzer direction are both in the plane of incidence and the analyzer slit is perpendicular to the plane of incidence. Au(111) and Ag(111) films on mica are cleaned by noble gas sputtering and annealing. Surface cleanliness is judged by low-energy electron diffraction and the quality of the electronic surface state in ARPES. Ultrathin CrSBr films are prepared using the KISS method [21]. In short, CrSBr crystals are cleaved in vacuum to obtain a clean surface and this is then gently pushed against the cleaned metal substrate surface, leaving ultrathin flakes on the substrate. The resulting flakes are studied by optical microscopy, atomic force microscopy, and ARPES. For additional experimental details, see Supplemental Material (SM) [24] including Ref. [25].

To theoretically describe the doped flakes, we apply density functional theory (DFT) calculations for bilayer samples taking the local Coulomb interaction into account on the mean-field level within DFT + U [26], using $U = 3.68$ eV and $J = 0.39$ eV as recently estimated from constrained random phase approximation calculations [18]. The charge transfer is modeled by artificially adding +0.125 electrons per layer, which is counteracted by a positively charged background. All calculations are spin-resolved and are performed within the Vienna *Ab Initio* Simulation Package [27,28] applying the generalized gradient approximation within PBE [29] and using $16 \times 12$ Monkhorst-Pack $k$ grids and an energy cutoff 500 eV, starting from a layered antiferromagnetic ordering. The lattice constants and atomic positions are relaxed until forces acting on individual atoms are smaller than 5 meV/Å whereby we take van der Waals effects into account [30,31] (for further details see SM [24]).

## III. RESULTS AND DISCUSSION

### A. Experiments

Figure 1(a) shows an optical microscopy image of a flake exfoliated on Au(111). The flake covers a large area of $\approx 800 \times 200$ μm$^2$. It is almost transparent, with dark holes in the substrate clearly visible through the flake [such holes are a typical defect for Au(111) on mica]. The thickness of the flake varies between 1 and 10 nm whereas flakes exfoliated on Ag(111) have a minimal thickness of 10 nm. The exact thickness does not seem to be critical because the observed electronic structure of the flakes does not vary across many preparations. In addition to the very thin flakes studied here, the microscopic images typically also show large and much thicker flakes with the characteristic rectangular shape of CrSBr crystals [19]. These appear black in the images and show the same charging effects in low-temperature ARPES that are also observed for bulk crystals [17,24].

A photoemission image of the same flake as in Fig. 1(a) is shown in Fig. 1(b), obtained by scanning the synchrotron radiation light spot across the sample while monitoring the photoemission intensity of Br 3d core levels. The flake is



FIG. 1. (a) Exfoliated ultrathin CrSBr flake on Au(111) seen by optical microscopy. (b) The same flake imaged by ARPES as the photoemission intensity of Br 3d core levels measured at 130 eV photon energy. (c) Photoemission intensity at the Fermi level for the same flake measured at 100 eV photon energy, showing a superposition of CrSBr and Au(111) features. The dashed lines mark the rectangular two-dimensional Brillouin zones of CrSBr. (d) Corresponding photoemission intensity at the Fermi level for a CrSBr flake deposited on Ag(111). The arrow indicates the band splitting at X, corresponding to Fig. 4(g).

clearly visible but its boundaries appear blurred. This is due to the rather large light spot footprint ($\approx 60 \times 120$ μm$^2$) that also leads to the CrSBr photoemission intensity always being observed together with that of the substrate.

The photoemission intensity at the Fermi level $E_F$ for ultrathin CrSBr flakes on Au(111) and Ag(111) is shown in Figs. 1(c) and 1(d), respectively. The CrSBr signal is easily distinguished from that of the substrates by symmetry alone. CrSBr has a rectangular unit cell and highly directional features corresponding to the expected periodicity are observed for both surfaces. The substrates, by contrast, give rise to the large hexagonal structures that represent cuts through the bulk Fermi surface. Observing a CrSBr Fermi contour implies that the flakes become metallic upon placing them on the substrates, creating an Ohmic contact. Note that the CrSBr features are aligned differently to the Au(111) and Ag(111) bulk Fermi surfaces. This alignment can be changed deliberately by choosing the desired relative orientation of the crystals in the KISS process. We do not observe any major changes of the CrSBr electronic structure as a function of relative CrSBr-substrate orientation, suggesting that the CrSBr-substrate interaction is dominated by screening and charge transfer rather than by hybridization or moiré potentials. Examples for differently oriented flakes are given in the SM [24].

FIG. 2. Photoemission intensity along high-symmetry lines for ultrathin CrSBr on Au(111) and Ag(111) collected with $h\nu = 56$ eV. (a), (b) Situation for Au(111) in the $x$ and $y$ direction, respectively. The conduction band minimum (CBM) and valence band maximum (VBM) are marked by arrows. The corresponding energies are indicated by horizontal lines. (c), (d) Corresponding data for Ag(111).

While the CrSBr flakes show quasi-1D Fermi contours on both substrates, the Fermi contour topology is surprisingly different. The origin of this can be understood by inspecting the dispersion of the CrSBr states for both substrates in the extended zone scheme in Fig. 2. Comparing the results along $\Gamma$-X in Figs. 2(a) and 2(c), it becomes clear that the electronic structure is similar on both substrates but the flakes are more strongly electron doped on Ag(111). An electronlike band (with a positive effective mass) is observed around the $\Gamma$ point of the Brillouin zone (BZ) for CrSBr on both Au(111) and Ag(111). It corresponds to the bulk conduction band minimum (CBM) of CrSBr, which is populated by charge transfer from the substrate. This band is more strongly populated on Ag(111). The binding energy maximum at $\Gamma$ is at $308 \pm 8$ and $187 \pm 8$ meV on Ag(111) and Au(111), respectively. This trend is consistent with the lower work function of Ag(111) leading to a stronger charge transfer [32,33] and it has also been observed for other 2D semiconductors [34].

The electronic structure difference between the two substrates goes beyond a doping-induced rigid shift of the bands. Indeed, it resembles a Lifshitz-type transition of the band structure, known earlier as electronic topological transition [35–38], and it even changes the fundamental band gap of the material. The evolution of the Fermi contours in Figs. 1(c) and 1(d) already shows the hallmark of Lifshitz transitions, namely, the disconnection of some Fermi contours and the appearance of others. The complexity of the changes can be fully appreciated when comparing the band structure change at the X point to that at $\Gamma$. For CrSBr on Au(111), the conduction band at X is barely populated with a maximum binding energy of $39 \pm 8$ meV. On Ag(111) the state is found at $317 \pm 8$ meV, corresponding to a much bigger shift than for the state at

$\Gamma$. Indeed, the shift is so big that the conduction band at X ends up (just) below that at $\Gamma$, turning CrSBr on Ag(111) into an indirect band gap semiconductor. Given the fact that a strong hybridization of CrSBr and substrate states appears unlikely due to symmetry and that we do not find experimental evidence for this either, it is tempting to ascribe this band structure change to the different doping levels. We will confirm this in the theoretical treatment below.

Already a superficial inspection of the Fermi contours in Figs. 1(c) and 1(d) appears to confirm the quasi-1D character of the CrSBr conduction band. For CrSBr/Au(111) the entire Fermi contour is comprised of the lowest conduction band. The contour is almost 1D, apart from the oval shape around $\Gamma$. On Ag(111), a second band above the CBM is partly populated, resulting in the photoemission maxima at the X points in Fig. 1(d). The lowest conduction band no longer crosses $E_F$ in the X direction. This is the reason for the open parallel lines in Fig. 1(d). The dispersion around the conduction band minimum at $\Gamma$ is highly anisotropic for both surfaces. This can be seen from the effective masses obtained by fitting the detailed dispersion. These are $0.73m_e$ ($0.28m_e$) and $1.3m_e$ ($0.2m_e$) for the $x(y)$ direction on Au(111) and Ag(111), respectively (see SM [24]). The rather big difference of the effective masses between the two substrates is not surprising but merely a manifestation of the nonrigid band structure changes upon doping.

The valence band maximum (VBM) is observed at the $\Gamma$ points for CrSBr flakes on both Au(111) and Ag(111) in Figs. 2(a) and 2(b) (marked by arrows). The VBM is not equally well observed for every $\Gamma$ point in the extended zone scheme. In particular, the band is completely absent for normal emission at $\Gamma_{00}$. This has also been observed for the VBM in bulk samples where it has been ascribed to sublattice interference effects [17]. The band gap at $\Gamma$ determined for CrSBr flakes on Au(111) and Ag(111) is $1.14 \pm 0.03$ eV and $1.18 \pm 0.02$ eV, respectively, which is much smaller than the theoretical bulk band gap of $\approx 2.1$ eV [17] and estimated bilayer band gap of $\approx 2.4$ eV (cf. bulk to bilayer trend in Ref. [16]). Thus, the different charge transfer-induced doping levels on Au(111) and Ag(111) affect the band gap by only $\approx 0.04$ eV. At this stage, it remains elusive if the metallic substrate screening, the doping-induced internal screening, or their combined effects are mainly responsible for the significantly reduced gap. Similar trends of gap reduction have been observed for other 2D semiconductors on metallic substrates [34,39,40].

Finally, Fig. 3 shows the CrSBr band structure for flakes on Au(111) for a temperature in the bulk paramagnetic regime (235 K). This is compared to low-temperature results along the same direction in reciprocal space. No significant differences are found apart from a general broadening at higher temperature and a slightly smaller doping, with the CBM moving up to $142 \pm 10$ meV at 235 K (obtained by fitting the entire dispersion around the high symmetry points, see SM [24]).

## B. Calculations

All of the experimental observations including their variations with substrates can be explained by comparison to
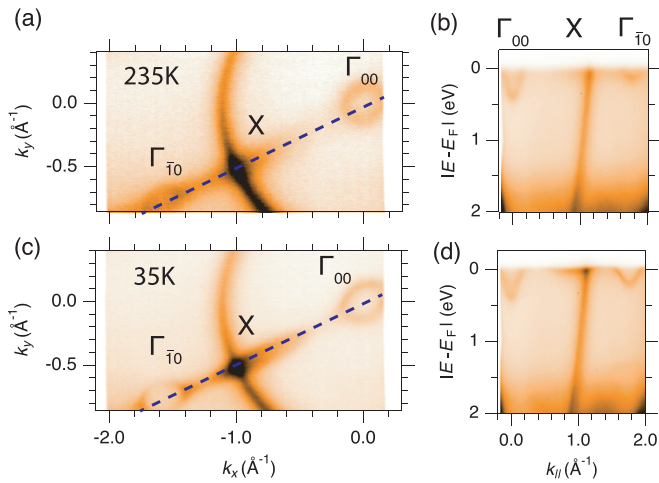
FIG. 3. Temperature-dependent ARPES measurements of ultra-thin CrSBr deposited on Au(111) with multiple rotational domains. (a) and (c) Photoemission intensity at the Fermi level at 235 K and 35 K, respectively. (b) and (d) Corresponding photoemission intensity dispersion along $\Gamma_{00}$-$\Gamma_{\bar{1}0}$.

our calculations. As a minimal model, we show bilayer band structures without doping, with electron doping, as well as with electron doping and under in-plane compressive strain in Figs. 4(a)–4(c). In all of these band structures we indicate the $d_{x^2-y^2}$ orbital weights from the outer and inner Cr atoms. Note that the undoped DFT + U results have been added only for reference. Without metallic substrates and the accompanying screening and charge transfer, DFT + U calculations are not reliable and, e.g., significantly underestimate the band gap [17]. The strained case has been added for further comparison, keeping in mind that the lattice constants from our

DFT + U calculations under electron doping might not be accurate. In the panels below the band structures we depict the accompanying Fermi contours to compare to the ARPES results. In all of these antiferromagnetic band structures, we find two strongly anisotropic Cr $d_{x^2-y^2/z^2}$-orbital-dominated lowest CBs, well separated from the other CBs and well-defined band gaps on the order of 1–1.3 eV. Especially the latter points towards the validity of the simplified DFT + U approach to describe our experimental results for thin CrSBr films on metallic substrate, which we understand as a result of the enhanced substrate and internal screening.

The DFT + U calculation for the undoped CrSBr bilayer in Fig. 4(a) significantly underestimates the direct band gap of about 1.3 eV at the $\Gamma$ point and the two CBs are nearly degenerate at X. The $d_{x^2-y^2}$ contributions from the inner and outer Cr atoms is mixed in both of the lowest CBs. In such a scenario, any finite doping (approximated by a rigid shift of the Fermi level into the CBs, as indicated by the dashed and dotted horizontal lines) reaching the X minimum would create two Fermi contours with a full pocket around X for intermediate doping, cf. Fig. 4(d).

Upon taking the charge transfer explicitly into account, the lower CB becomes dominated by the outer Cr $d_{x^2-y^2}$ weight and the second CB by the inner Cr $d_{x^2-y^2}$ weight. As a result we find a small charge accumulation disproportionation between these Cr atoms and the inner and outer Cr atoms now host slightly different magnetic moments. In this case, the approx. 90° angles of the outer Cr-Br-Cr bridge is approximately 1° smaller than the angle of the inner bridge. As a result of this intralayer magnetic symmetry breaking, the degeneracy at X is lifted, as shown in Fig. 4(b). The resulting splitting is directly observable in the Fermi contour as soon as the second band at X gets occupied, see transition between Figs. 4(f) and 4(g).
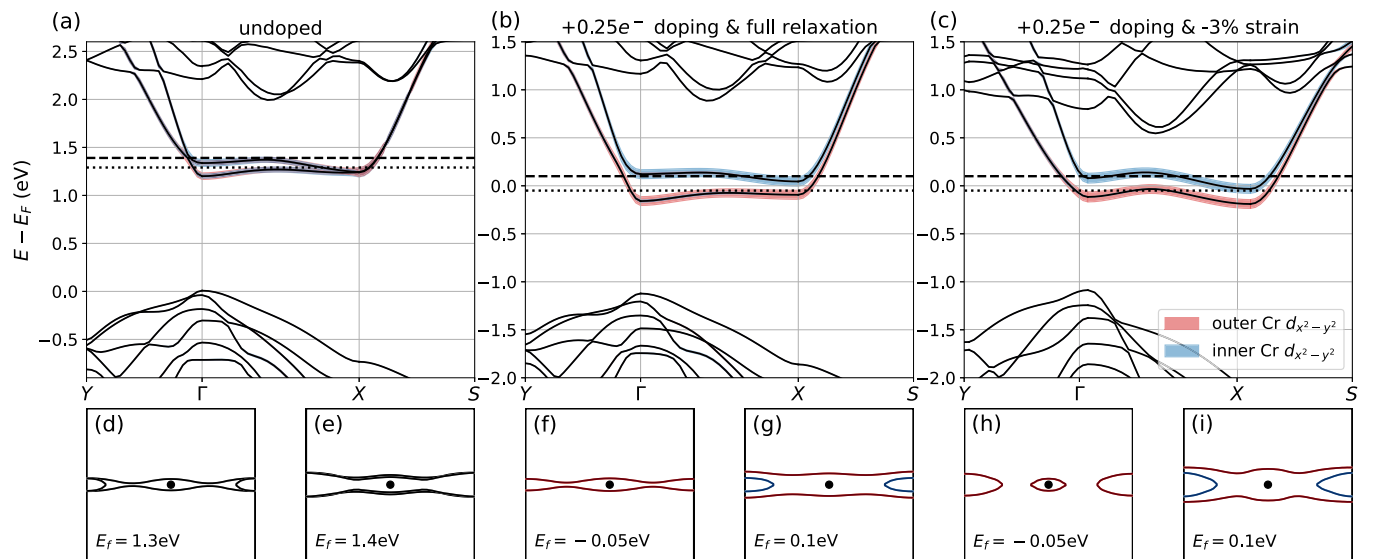


FIG. 4. CrSBr bilayer DFT + U band structures and Fermi contours. (a) Band structures without doping (for reference); (b) with a doping of +0.125 electron per layer; (c) with doping and applying in-plane compressive strain. Red and blue indicate the $d_{x^2-y^2}$ orbital contributions of the outer and inner Cr atoms, respectively. (d) to (i) Effective Fermi contours resulting from these band structures according to the chemical potentials indicated by the dashed and dotted lines and the labels. In the doped cases the indicated chemical potentials are shifted by −0.05 and +0.1 eV with respect to the DFT + U predicted $E_F$ to further illustrate the effects of modifications to the doping. Red and blue Fermi surface contours only indicate the lower and upper CB origin and do not refer to the Cr $d_{x^2-y^2}$ contribution.

Finally, upon applying an in-plane strain of $-3\%$, we see that the bands between $\Gamma$ and X become more dispersive and the CB minimum shifts to X yielding an indirect band gap. In this case, a small chemical potential change can result in two fully detached pockets around $\Gamma$ and X, as indicated in Fig. 4(h). Increasing the chemical potential gives again rise to a tubelike Fermi contour together with a detached second pocket around X, as shown in Fig. 4(i).

Our theoretical results and especially their variations upon changing the chemical potential are in good qualitative agreement with the experimental findings. For the Au(111) supported flakes, a very low doping level is present with the CBM at $\Gamma$ being clearly occupied and the remaining CB straddling $E_F$. This is similar to the situation in Figs. 4(d) and 4(f) but there is no possibility to establish if the two bands at X are degenerate or not. For CrSBr flakes on Ag(111), on the other hand, the higher doping shows clear evidence of a band splitting at X, as seen, e.g., by the similarity of the calculated Fermi contours in Figs. 4(g) and 4(i) and the experimental one in Fig. 1(d) where the splitting is indicated by an arrow. This splitting underlines that the doping of ultrathin CrSBr does not just lead to a rigid displacement of the Fermi level but leads to a Lifshitz transition accompanied by the breaking of the intralayer magnetic symmetry. Finally, the experimentally observed relocation of the absolute CBM from $\Gamma$ to X could be achieved by a small strain of the CrSBr film or be a small doping-dependent change of the equilibrium lattice constant. Note that a rather high compressive strain has been chosen here to exaggerate the relative shifts between the CB minima at $\Gamma$ and X.

The most interesting qualitative difference between our theoretical band structures and the experimental ARPES data is the rather deep electron pocket around $\Gamma$. Our DFT $+$ U calculations cannot fully reproduce these characteristics, which might hint towards further band structure renormalization beyond the mean-field ones discussed here, such as electron-plasmon or electron-magnon coupling or further lattice structure renormalization effects.

## IV. CONCLUSIONS

In conclusion, upon investigating ultrathin CrSBr flakes on Au(111) and Ag(111) substrates with clean interfaces obtained by *in situ* exfoliation, we could systematically study the effects of charge transfer from the metallic substrates to the CrSBr layers. We found that this charge transfer induces nonrigid shifts and Lifshitz-like transitions in the CrSBr conduction bands. At small doping levels, we find a quasi-1D Fermi contour with an anisotropic electron pocket around $\Gamma$, while at large doping the Lifshitz transition yields a full and nonclosed tubelike pocket expanding through the entire Brillouin zone, accompanied by a second fully detached pocket around X. The comparison to mean-field DFT $+$ U calculations including the effects of charge transfer allows us to interpret these characteristics as the result of an intralayer magnetic symmetry breaking. The latter is resulting from the different magnetic properties of the inner and outer CrSBr layers in stacks with finite number of layers. As such these kind of magnetic symmetry breaking effects could be expected in various other materials as well as under different doping scenarios and need to be considered case by case.

[1] N. D. Mermin and H. Wagner, Phys. Rev. Lett. **17**, 1133 (1966).

[2] S. Chakravarty, B. I. Halperin, and D. R. Nelson, Phys. Rev. B **39**, 2344 (1989).

[3] *Magnetic Properties of Layered Transition Metal Compounds* edited by L. J. de Jongh (Springer, Berlin, 1990).

[4] V. Y. Irkhin, A. A. Katanin, and M. I. Katsnelson, Phys. Rev. B **60**, 1082 (1999).

[5] M. Gibertini, M. Koperski, A. F. Morpurgo, and K. S. Novoselov, Nat. Nanotechnol. **14**, 408 (2019).

[6] K. Zollner, P. E. Faria Junior, and J. Fabian, Phys. Rev. B **100**, 085128 (2019).

[7] B. Huang, G. Clark, E. Navarro-Moratalla, D. R. Klein, R. Cheng, K. L. Seyler, D. Zhong, E. Schmidgall, M. A. McGuire, D. H. Cobden *et al.*, Nature (London) **546**, 270 (2017).

[8] C. Gong, L. Li, Z. Li, H. Ji, A. Stern, Y. Xia, T. Cao, W. Bao, C. Wang, Y. Wang *et al.*, Nature (London) **546**, 265 (2017).

[9] Y. Deng, Y. Yu, Y. Song, J. Zhang, N. Z. Wang, Z. Sun, Y. Yi, Y. Z. Wu, S. Wu, J. Zhu *et al.*, Nature (London) **563**, 94 (2018).

[10] O. Göser, W. Paul, and H. Kahle, J. Magn. Magn. Mater. **92**, 129 (1990).

[11] E. J. Telford, A. H. Dismukes, K. Lee, M. Cheng, A. Wieteska, A. K. Bartholomew, Y.-S. Chen, X. Xu, A. N. Pasupathy, X. Zhu *et al.*, Adv. Mater. **32**, 2003240 (2020).

[12] Y. Guo, Y. Zhang, S. Yuan, B. Wang, and J. Wang, Nanoscale **10**, 18036 (2018).

[13] Z. Jiang, P. Wang, J. Xing, X. Jiang, and J. Zhao, ACS Appl. Mater. Interfaces **10**, 39032 (2018).

[14] C. Wang, X. Zhou, L. Zhou, N.-H. Tong, Z.-Y. Lu, and W. Ji, Sci. Bull. **64**, 293 (2019).

[15] N. P. Wilson, K. Lee, J. Cenker, K. Xie, A. H. Dismukes, E. J. Telford, J. Fonseca, S. Sivakumar, C. Dean, T. Cao *et al.*, Nat. Mater. **20**, 1657 (2021).

[16] J. Klein, B. Pingault, M. Florian, M.-C. Heißenbüttel, A. Steinhoff, Z. Song, K. Torres, F. Dirnberger, J. B. Curtis, M. Weile *et al.*, ACS Nano **17**, 5316 (2023).

[17] M. Bianchi, S. Acharya, F. Dirnberger, J. Klein, D. Pashov, K. Mosina, Z. Sofer, A. N. Rudenko, M. I. Katsnelson, M. van Schilfgaarde *et al.*, Phys. Rev. B **107**, 235107 (2023).

[18] A. N. Rudenko, M. Rösner, and M. I. Katsnelson, npj Comput. Mater. **9**, 83 (2023).

[19] J. Klein, T. Pham, J. D. Thomsen, J. B. Curtis, T. Denneulin, M. Lorke, M. Florian, A. Steinhoff, R. A. Wiscons, J. Luxa *et al.*, Nature Commun. **13**, 5420 (2022).

[20] E. J. Telford, A. H. Dismukes, R. L. Dudley, R. A. Wiscons, K. Lee, D. G. Chica, M. E. Ziebel, M.-G. Han, J. Yu, S. Shabani *et al.*, Nature Mater. **21**, 754 (2022).

[21] A. Grubišić-Čabo, M. Michiardi, C. E. Sanders, M. Bianchi, D. Curcio, D. Phuyal, M. H. Berntsen, Q. Guo, and M. Dendzik, Adv. Sci. **10**, 2301243 (2023).

[22] J. Strasdas, B. Pestka, M. Rybak, A. K. Budniak, N. Leuth, H. Boban, V. Feyer, I. Cojocariu, D. Baranowski, J. Avila *et al.*, Nano Lett. (2023), doi: 10.1021/acs.nanolett.3c02906.

[23] S. V. Hoffmann, C. Søndergaard, C. Schultz, Z. Li, and P. Hofmann, Nucl. Instrum. Methods Phys. Res., Sect. A **523**, 441 (2004).

[24] See Supplemental Material at http://link.aps.org/supplemental/10.1103/PhysRevB.108.195410 for additional details on sample preparation, ARPES data, and calculational results for doping-dependent structure and magnetic anisotropy.

[25] I. A. Nechaev, M. F. Jensen, E. D. L. Rienks, V. M. Silkin, P. M. Echenique, E. V. Chulkov, and P. Hofmann, Phys. Rev. B **80**, 113402 (2009).

[26] A. I. Liechtenstein, V. I. Anisimov, and J. Zaanen, Phys. Rev. B **52**, R5467 (1995).

[27] G. Kresse and J. Furthmüller, Comput. Mat. Sci. **6**, 15 (1996).

[28] G. Kresse and J. Furthmüller, Phys. Rev. B **54**, 11169 (1996).

[29] J. P. Perdew, K. Burke, and M. Ernzerhof, Phys. Rev. Lett. **77**, 3865 (1996).

[30] J. Klimeš, D. R. Bowler, and A. Michaelides, J. Phys.: Condens. Matter **22**, 022201 (2010).

[31] J. Klimeš, D. R. Bowler, and A. Michaelides, Phys. Rev. B **83**, 195131 (2011).

[32] G. V. Hansson and S. A. Flodström, Phys. Rev. B **18**, 1572 (1978).

[33] M. Chelvayohan and C. H. B. Mee, J. Phys. C **15**, 2305 (1982).

[34] M. Dendzik, A. Bruix, M. Michiardi, A. S. Ngankeu, M. Bianchi, J. A. Miwa, B. Hammer, P. Hofmann, and C. E. Sanders, Phys. Rev. B **96**, 235440 (2017).

[35] I. Lifshitz, Sov. Phys. JETP **11**, 1130 (1960).

[36] I. Lifshits, M. Azbel, and M. Kaganov, *Electron Theory of Metals* (Consultants Bureau, New York, 1973).

[37] Y. Blanter, M. Kaganov, A. Pantsulaya, and A. Varlamov, Phys. Rep. **245**, 159 (1994).

[38] M. I. Katsnelson, I. I. Naumov, and A. V. Trefilov, Phase Transitions **49**, 143 (1994).

[39] P. Eickholt, C. Sanders, M. Dendzik, L. Bignardi, D. Lizzit, S. Lizzit, A. Bruix, P. Hofmann, and M. Donath, Phys. Rev. Lett. **121**, 136402 (2018).

[40] A. Grubišić Čabo, J. A. Miwa, S. S. Grønborg, J. M. Riley, J. C. Johannsen, C. Cacho, O. Alexander, R. T. Chapman, E. Springate, M. Grioni *et al.*, Nano Lett. **15**, 5883 (2015).